Commun Nonlinear Sci Numer Simulat 90 (2020) 105390

Contents lists available at ScienceDirect

Commun Nonlinear Sci Numer Simulat

journal homepage: www.elsevier.com/locate/cnsns

Research paper

Chaotic dynamics in a neural network with different types of external stimuli☆

Hairong Lin, Chunhua Wang*, Wei Yao, Yumei Tan

College of Computer Science and Electronic Engineering, Hunan University, Changsha 410082, China

ARTICLE INFO

Article history:
Received 7 January 2020
Revised 18 May 2020
Accepted 3 June 2020
Available online 6 June 2020

Keywords:
Hopfield neural network
Multi-scroll chaotic attractors
Electromagnetic stimulus
Hamilton energy

ABSTRACT

Biological nervous system is very sensitive to external disturbances, and appropriate stimulus is beneficial for improving neural function in the neural system. In this paper, the effect of different external stimuli on chaotic dynamics in a Hopfield neural network with three neurons is explored. Mathematical model of the neural network is respectively established under three different cases, namely without external stimulus, with only electromagnetic radiation stimulus, and with both electromagnetic radiation stimulus and multi-level-logic pulse stimulus. Under the three cases, equilibrium points, stabilities, and attractors of the neural network are investigated carefully. The research results demonstrate that the neural network with periodic attractors can induce abundant chaotic attractors by imposing electromagnetic radiation on its one neuron. And when this neuron is simultaneously stimulated via electromagnetic radiation and multi-level-logic pulse, the neural network can produce complex multi-scroll attractors previously unobserved in Hopfield-type neural networks. Numerical results are verified by hardware experiments, effectively. Furthermore, based on the Helmholtzâs theorem, the Hamilton energy of the neural network is calculated and analyzed. It is found that lower average Hamilton energy can be detected in the neural network when complexity of external stimuli is enhanced. These new findings could offer a new insight into the occurrence mechanism of some neurological diseases.

1. Introduction

Neural system which comprises a great mass of biological neurons interconnected is regarded as one of the most intricate networks in nature. Numerous physical and biological experiments corroborated that various dynamical phenomena associated with neural function can be observed in the neural systems [1–3]. Especially, some neurological diseases like Epilepsy [4], Psychosis [5] and Alzheimer [6] are closely related to the dynamics of the neural system [7–9]. Consequently, the investigation of chaotic dynamics in neural networks is great significance for the precaution and treatment of nervous diseases.

Attractor is a nonlinear dynamical phenomenon, and widely exists in various nature fields such as biological systems [10–12], physical engineering [13,14] and material science [15]. From the perspective of generation mechanism of attractors,

☆ This project is supported by The Major Research Project of National Natural Science Foundation of China (No.91964108), The National Natural Science Foundation of China (No.61971185) and The Open Fund Project of Key Laboratory in Hunan Universities (No.18K010).

* Corresponding author.
E-mail addresses: haironglin66@126.com (H. Lin), wch1227164@hnu.edu.cn (C. Wang).

https://doi.org/10.1016/j.cnsns.2020.105390
1007-5704/

it can be divided into self-excited attractors [16] and hidden attractors [17,18]. From the view of Lyapunov exponents, it can be divided into periodic attractors, transient chaotic attractors [19], chaotic attractors and hyperchaotic attractors [20,21]. And from an attractor structure point of view, attractor contains single-scroll attractors and multi-scroll attractors [22–24]. Since the multi-scroll attractors have more complex dynamics than single-scroll attractors [25–27], the generation and implementation of multi-scroll attractors have become a hot topic in the research of nonlinear dynamical systems. For example, Yu et al. [28] designed and implemented *n*-scroll attractors in a general Jerk circuit by introducing a nonlinear modulating function. Hu et al. [29] affirmed that an improved Sprott A system can generate hidden multi-scroll attractors based on a simple sine function. And Hong et al. [30] substantiated the Lorenz system can produce the multi-scroll attractors by using multi-level-logic pulse excitation technique. Additionally, the original Chua′s system can generate multi-scroll attractors by introducing a multi-piecewise quadratic nonlinear memristor [31]. Indeed, most dynamical systems can easily generate multi-scroll attractors by introducing appropriate nonlinear functions with multiple breakpoints. However, this approach is not suitable for generating multi-scroll attractors in neural network models, because these nonlinear functions have no any physical interpretations. As a result, the multi-scroll attractor has not been observed in the neural network models so far.

Hopfield neural network abstracted from human brain is a crucial neural network model in artificial neural network territory [32,33]. Due to the prominent nonlinearity of neuron activation function, the Hopfield neural network is often used to emulate the intricate chaotic dynamics of the brain [34,35]. Over the past few decades, a variety of dynamical attractors including chaotic attractors [36–38], hyperchaotic attractors [39] and hidden chaotic attractors [40] have been detected in some small Hopfield neural networks. Especially, in recent years, some scholars discovered that more complicated chaotic attractors can be engendered in some memristive Hopfield neural networks through introducing a memristor as a neural synapse. For instance, Bao et al. [41] demonstrated coexisting asymmetric chaotic attractors can be obtained in the neural network with a hyperbolic-type memristor synapse. Chen et al. [42,43] proved that the memristor synapse-coupled neural network with two neurons can display multiple coexisting chaotic attractors. And Li et al. [44] revealed coexisting hyperchaotic attractors in a small memristive neural network. What is more, Pham et al. [45] found hidden hyperchaotic attractors in a memristive neural network with three neurons.

In fact, dynamics of a neuron or a neural network can be affected by several external stimuli like magnetic field and electric field. Li et al. [46] firstly found that electromagnetic radiation can inhibit electrical activities of neurons and regulate collective dynamics of neural networks. Etémé et al. have explored various dynamical phenomena including firing and synchronization modes [47], unstable discrete modes [48], elimination of spiral waves [49] and long-range memory effects [50] in single neuron model under magnetic field effect. And Ma et al. [51] confirmed that electric field stimulus can induce mode transition in electrical activities of isolated neuron. Additionally, some neuroscientists have found that bipolar pulse current stimulus can cause complex coexisting firing in two-dimensional Hindmarsh Rose neuron model [52]. Multi-level-logic pulse consisted with of multiple bipolar pulse has more rich frequency and amplitude components, which is more perfectly emulating an electric field stimulus effect on the neural networks. Although the influence of single neuron under magnetic field stimulus or electric field stimulus has been widely investigated, the neural networks affected by magnetic field and electric field are rarely studied. Moreover, such external stimuli on neural networks have not been explored from the view of energy.

As we all know, energy plays a key role in the information encoding and processing of biological nervous system [53,54], as an example, normal electric activities in neural system need energy supplying. According to the Helmholtzâs theorem [55], the Hamilton energy of dynamical systems can be calculated [56–58]. As a consequence, some researchers suggested that Hamilton energy can be estimated in neuron and neural network models by using Helmholtzâs theorem. And energy analysis can give helpful clues to understand electrical activities and information encoding in neurons. For example, Song et al. [59] confirmed that the firing pattern of neuron is connected with the energy release, and bursting and chaotic firing in neuron can present lower Hamilton energy. Wang et al. [60] believed that the Hamilton energy of neuron is closely related to its firing modes instead of the external forcing currents. Moreover, Wu et al. [61] unveiled that the transition of firing mode in neuron is dependent on the exchange of electric field energy and magnetic field energy, and found that field coupling consumes lower energy than electrical synapse coupling in neural network. As mentioned in the previous works, the neuronal network can give appropriate responses to energy from electric field and magnetic field. And from the view of dynamical control, external nonlinear functions can input continuous energy to change the dynamical states in dynamical systems. Indeed, there is evidence that the chaotic dynamics of the neural network can be changed by external stimulus effectively [46,47]. Recently, Hu et al. [62] showed that a Hopfield neural network with three neurons subjected to external electromagnetic radiation can produce chaotic attractors, hidden chaotic attractors and transient chaotic attractors. Similarly, Lin et al. [63] confirmed that hidden extremely multistability with hyperchaotic attractors and transient chaotic attractor can be observed in a small Hopfield neural network under electromagnetic radiation. Additionally, Lin and Wang [64] studied the chaotic dynamics of the Hopfield neural network with n neurons under electromagnetic radiation. It is found that the dynamical behaviors of the neural network become more and more complex with the increasing of the number of neurons affected by external electromagnetic radiation. However, by now, the effects of different types of external stimuli, for example, no external stimulus, only electromagnetic radiation stimulus, both electromagnetic radiation and multi-level-logic pulse stimulus, on the chaotic dynamics in neural networks have not been explored.

In this work, we study the chaotic dynamics of the neural network under three different cases, namely without external stimulus, only electromagnetic radiation stimulus, with both electromagnetic radiation and multi-level-logic pulse stimuli. Firstly, the mathematical models of the neural network in the three situations are established, and their equilibrium points

and corresponding stabilities are orderly analyzed and discussed. Afterwards, the dynamical attractors of the neural network under different cases are numerically investigated by adopting phase plots, bifurcation diagrams, Lyapunov exponents and Poincaré maps. We show that the neural network with periodic attractors can induce abundant chaotic attractors by putting electromagnetic radiation on its one neuron. And complex multi-scroll attractors including double-scroll attractor, four-scroll attractor and six-scroll attractor can be observed in the neural network stimulated by electromagnetic radiation and multi-level-logic pulse simultaneously, which has not been reported in the previous works for the Hopfield type neural system. In addition, the Hamilton energy function of the neural network is calculated and its energy transition is discussed. It is found that the energy in neural system is mainly dependent on its dynamical behaviors rather than external stimuli, and the multi-scroll attractors enjoy lower average Hamilton energy. Finally, the numerical simulation results are verified by circuital neural network which is realized by using analog electric devices.

The rest of this article is arranged as follows. In Section 2, the neural network is modeled under three different cases, and their equilibrium points and corresponding stabilities are analyzed. The chaotic dynamics of the neural network in the three cases are respectively researched in Section 3. Section 4 discussed the Hamilton energy of the neural network. Hardware experiments based on the designed neural circuit are implemented in Section 5. The last Section, namely Section 6 summarizes the full text.

2. A neural network under different external stimuli

2.1. Scene modeling

Hopfield neural network which defines a similar network structure to the biological neural system provides a reliable model to imitate dynamics of brain activities. A original Hopfield neural network which is made up of n neurons can be described by Hopfield [32], Lin and Wang [64]

$$C_i\dot{x}_i = -x_i/R_i + \sum_{j=1}^{n} w_{ij}\tanh(x_i) + I_i(i, j \in N^*), \tag{1}$$

where C_i, R_i, and x_i are the capacitance, resistance, and voltage between the outside and inside of the cell membrane of the neuron i, respectively. $\tanh(x_i)$ is the neuron activation function, and w_{ij} is the synaptic weight value describing the connection strength between neuron i and neuron j [65]. Besides, I_i is bias current, which is usually equal to zero.

(1) Case 1: the neural network without external stimulus

Based on the original neural network model (1), a small neural network with three neurons is proposed by selecting appropriate synaptic weight values, and its expression is given by

$$\begin{cases} C_1\dot{x}_1 = -x_1/R_1 + 1.5\tanh(x_1) + 2\tanh(x_2) + 0.9\tanh(x_3) + I_1 \\ C_2\dot{x}_2 = -x_2/R_2 - 1.5\tanh(x_1) + 1.5\tanh(x_2) - 0.45\tanh(x_3) + I_2 \\ C_3\dot{x}_3 = -x_3/R_3 + 3\tanh(x_1) - 2\tanh(x_2) + 1.5\tanh(x_3) + I_3 \end{cases} \tag{2}$$

Assuming $C_1 = C_2 = C_3$=1, $R_1 = R_2 = R_3$=1, $I_1 = I_2 = I_3$=0, the presented neural network can be modeled as follows:

$$\begin{cases} \dot{x}_1 = -x_1 + 1.5\tanh(x_1) + 2\tanh(x_2) + 0.9\tanh(x_3) \\ \dot{x}_2 = -x_2 - 1.5\tanh(x_1) + 1.5\tanh(x_2) - 0.45\tanh(x_3) \\ \dot{x}_3 = -x_3 + 3\tanh(x_1) - 2\tanh(x_2) + 1.5\tanh(x_3) \end{cases} \tag{3}$$

1. Case 2: the neural network under electromagnetic radiation

It is well known that the influence of electromagnetic radiation on isolated neuron can be described by fluctuation of magnetic flux across cell membrane, and the coupling between magnetic flux and membrane voltage can be realized through using a flux-controlled memristor [66,67]. Usually, the flux-controlled memristor can be expressed by

$$\begin{cases} i = W(\varphi)v \\ \dot{\varphi} = v \\ W(\varphi) = \alpha + 3\beta\varphi^2 \end{cases}, \tag{4}$$

where i, v, φ are output current, input voltage, and magnetic flux, respectively. W(φ) denotes the memory conductance, and α, β are two memristor parameters. When we consider that the neuron 2 is influenced by electromagnetic radiation, the model of the neural network under electromagnetic radiation can be built as follows: [62,63]

$$\begin{cases} \dot{x}_1 = -x_1 + 1.5\tanh(x_1) + 2\tanh(x_2) + 0.9\tanh(x_3) \\ \dot{x}_2 = -x_2 - 1.5\tanh(x_1) + 1.5\tanh(x_2) - 0.45\tanh(x_3) + \rho x_2(\alpha + 3\beta\varphi^2) \\ \dot{x}_3 = -x_3 + 3\tanh(x_1) - 2\tanh(x_2) + 1.5\tanh(x_3) \\ \dot{\varphi} = \mu x_2 - \varepsilon\varphi \end{cases}, \tag{5}$$

where φ denotes the magnetic flux across cell membrane of the neuron 2. The term $\rho x_2(\alpha + 3\beta\varphi^2)$ is an induction current caused by the change of magnetic flux and field, where ρ represents the intensity of the electromagnetic induction. The term μx_2 is the changes of magnetic flux caused by membrane potential, and the term $\varepsilon\varphi$ is the leakage of magnet flux.

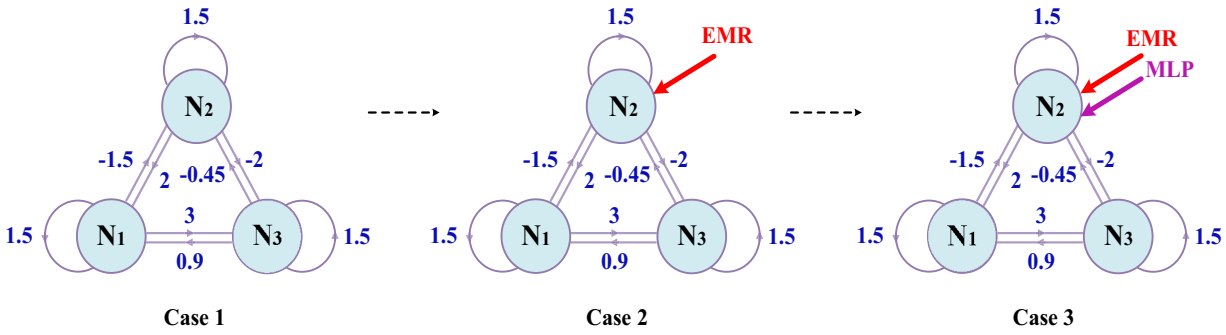

Fig. 1. Concept map of the neural network in different external stimulus cases

1. Case 3: the neural network under electromagnetic radiation and multi-level-logic pulse

To further explore the effects of different kinds of external stimuli on the chaotic dynamics of the neural network, electromagnetic radiation and multi-level-logic pulse signal are imposed on the neuron 2 simultaneously, where the multi-level-logic pulse signal can be described by [30]

$$I_{\mathrm{MLP}} = \sum_{1}^{n} a_n \mathrm{sign}(\sin(\omega_n t)), \tag{6}$$

where a_n, ω_n are pulse signal amplitude and frequency respectively. The model of the neural network under electromagnetic radiation and multi-level-logic pulse can be established as follows:

$$\begin{cases} \dot{x_1} = -x_1 + 1.5\tanh(x_1) + 2\tanh(x_2) + 0.9\tanh(x_3) \\ \dot{x_2} = -x_2 - 1.5\tanh(x_1) + 1.5\tanh(x_2) - 0.45\tanh(x_3) + \rho x_2(\alpha + 3\beta\varphi^2) + I_{\mathrm{MLP}} \\ \dot{x_3} = -x_3 + 3\tanh(x_1) - 2\tanh(x_2) + 1.5\tanh(x_3) \\ \dot{\varphi} = \mu x_2 - \varepsilon\varphi \end{cases} \tag{7}$$

Furthermore, to better understand these three cases, a corresponding concept map is delineated in Fig. 1, where N_1, N_2 and N_3 are three neurons, EMR represents electromagnetic radiation, and MLP represents multi-level-logic pulse.

2.2. Stability analysis

The equilibrium points of the neural network and their stabilities in the three cases are analyzed by graphic and numerical analytic methods. For case 1, by equating the left side of model (3) to 0, the equilibrium points can be solved by

$$E(x, y, z),\ (x = -y + 3.5\tanh(y) + 0.45\tanh(z)), \tag{8}$$

where the values of y and z can be solved by graphic analytic method. The following functions are obtained by substituting Eq. (8) to Eq. (3)

$$F_1(y, z) = -y - 1.5\tanh(-y + 3.5\tanh(y) + 0.45\tanh(z)) + 1.5\tanh(y) - 0.45\tanh(z), \tag{9}$$

$$F_2(y, z) = -z + 3\tanh(-y + 3.5\tanh(y) + 0.45\tanh(z)) - 2\tanh(y) + 1.5\tanh(z). \tag{10}$$

The functions (9) and (10) are numerically drawn in Fig. 2(a). Obviously, there is only one zero equilibrium point in the model (3). The stability of zero equilibrium point $E(0,0,0)$ can be determined by the eigenvalues of the following Jacobian matrix:

$$J_E = \begin{bmatrix} \frac{\partial \dot{x_1}}{\partial x_1} & \frac{\partial \dot{x_1}}{\partial x_2} & \frac{\partial \dot{x_1}}{\partial x_3} \\ \frac{\partial \dot{x_2}}{\partial x_1} & \frac{\partial \dot{x_2}}{\partial x_2} & \frac{\partial \dot{x_2}}{\partial x_3} \\ \frac{\partial \dot{x_3}}{\partial x_1} & \frac{\partial \dot{x_3}}{\partial x_2} & \frac{\partial \dot{x_3}}{\partial x_3} \end{bmatrix} = \begin{bmatrix} 0.5 & 2 & 0.9 \\ -1.5 & 0.5 & -0.45 \\ 3 & -2 & 0.5 \end{bmatrix}. \tag{11}$$

J_E has a characteristic equation:

$$|\lambda E - J_E| = (\lambda - 0.5)\left(\lambda^2 - \lambda - 0.35000516\right). \tag{12}$$

Solving the characteristic equation, we can get three eigenvalues λ_1=0.5, λ_2=1.2746 and λ_3=0.2746, respectively. Therefore, the zero equilibrium point of the neural network model (3) is an unstable node.

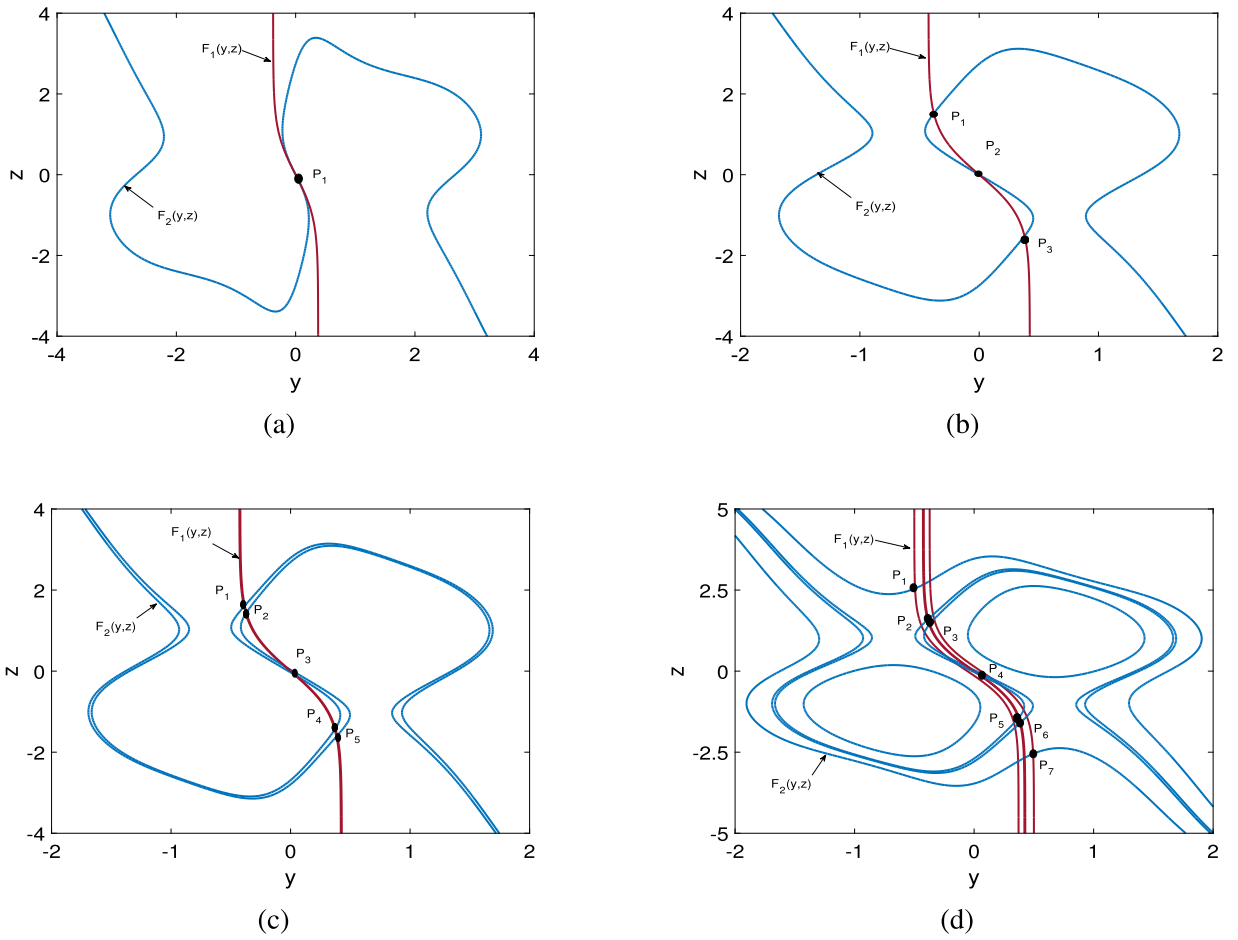

Fig. 2. Intersections determined by two functions where the curves of functions $F_1(y, z)$ and $F_2(y, z)$ are colored in dark red and dark blue, respectively, and $P_i(y, z)$ denotes the coordinates y and z in equilibrium point $E_i(x, y, z, w)$. (a) $F_1(y, z)$ in (9) and $F_2(y, z)$ in (10), (b) $F_1(y, z)$ in (15) and $F_2(y, z)$ in (16), (c) $F_1(y, z)$ in (20) and $F_2(y, z)$ in (21) with n=1, (d) $F_1(y, z)$ in (20) and $F_2(y, z)$ in (21) with n=2.

For case 2, through setting the left side of the model (5) equal to zero, its solutions can be determined as equilibrium points $\pm E_i(x, y, z, w)$, which can be calculated by

$$E_i(x, y, z, w)=(x, y, z, (\mu/\varepsilon)y), \tag{13}$$

where

$$x=-y+3.5\tanh(y)+0.45\tanh(z)+\rho y(\alpha+3\beta(\mu/\varepsilon)^2y^2)). \tag{14}$$

Here, the point (y, z) is the intersection coordinate of the following two functions

$$\begin{aligned} F_1(y,z) = &-y-1.5\tanh(-y+3.5\tanh(y)+0.45\tanh(z)+\rho y(\alpha+3\beta(\mu/\varepsilon)^2y^2)) \\ &+1.5\tanh(y)-0.45\tanh(z)+\rho y(\alpha+3\beta(\mu/\varepsilon)^2y^2) \end{aligned}, \tag{15}$$

$$F_2(y,z) = -z+3\tanh(-y+3.5\tanh(y)+0.45\tanh(z)+\rho y(\alpha+3\beta(\mu/\varepsilon)^2y^2))-2\tanh(y)+1.5\tanh(z). \tag{16}$$

When parameters are fixed as α=1.519, β=-0.04, ρ=-0.5, μ=0.1 and ε=0.45, the functions (15) and (16) are drawn in Fig. 2(b), synchronously. In Fig. 2(b), there are three intersections, namely P_1(-0.3799, 1.5195), P_2(0,0) and P_3(0.3799, -1.5195), respectively. Meanwhile, the values of x and w can be given by Eqs. (13) and (14). Hence three equilibrium points E_1(-0.1919,-0.3799,1.5195,-0.0084), E_2(0,0,0,0) and E_3(0.1919,0.3799,-1.5195,0.0084) can be attained from the Eq. (13). The Jacobian matrix of the model (5) on the equilibrium point $E(x, y, z, w)$ can be easily expressed as follows

$$J=\begin{bmatrix} -1+1.5sech^2(x) & 2sech^2(y) & 0.9sech^2(z) & 0 \\ -1.5sech^2(x) & -1+1.5sech^2(y)+\rho(\alpha+3\beta w^2) & -0.45sech^2(z) & 6\rho\beta yw \\ 3sech^2(x) & -2sech^2(y) & -1+1.5sech^2(z) & 0 \\ 0 & \mu & 0 & -\varepsilon \end{bmatrix}. \tag{17}$$

Based on Eq. (17), the eigenvalues of the equilibrium points E_1 and E_3 are λ_1=-0.45, λ_2=-0.8568, $\lambda_3 = \lambda_4$= 0.0539 ± 1.3473i. And the eigenvalues of the equilibrium point E_2 are λ_1=-0.45, λ_2=1.6907, $\lambda_3 = \lambda_4$=-0.4751 ± 0.8783i. Clearly, E_1 and E_3 are two unstable saddle focuses, and E_2 is an unstable saddle point. That is to say, external electromagnetic radiation can induce the changes of the equilibrium points in the neural network.

For case 3, by setting the left side of the model (7) to 0, its equilibrium points can be solved. And the solutions can be divided into two situations.

Situation 1:when $\omega_n t = k\pi\,(k \in N)$, I_{MLP}=0.

Under this situation, the model (7) and model (5) have the same equilibrium points and stabilities.

Situation 2: when $\omega_n t \neq k\pi (k \in N)$, $I_{MLP} = \sum_1^n \pm a_n$.

Under this situation, the equilibrium points of model (7) can be determined as follows:

$$E_i(x, y, z, w)=(x, y, z, (\mu/\varepsilon)y), \tag{18}$$

where

$$x= -y + 3.5\tanh(y) + 0.45\tanh(z) + \rho y(\alpha + 3\beta(\mu/\varepsilon)^2y^2)) + \sum_1^n (\pm a_n), \tag{19}$$

where the values of y and z can be solved by following two functions

$$\begin{aligned} F_1(y,z) = &-y - 1.5\tanh(-y + 3.5\tanh(y) + 0.45\tanh(z) + \rho y(\alpha + 3\beta(\mu/\varepsilon)^2y^2) + \sum_1^n (\pm a_n)) \\ &+1.5\tanh(y) - 0.45\tanh(z) + \rho y(\alpha + 3\beta(\mu/\varepsilon)^2y^2) + \sum_1^n (\pm a_n) \end{aligned}, \tag{20}$$

$$\begin{aligned} F_2(y,z) = &-z + 3\tanh(-y + 3.5\tanh(y) + 0.45\tanh(z) + \rho y(\alpha + 3\beta(\mu/\varepsilon)^2y^2) + \sum_1^n (\pm a_n)) \\ &-2\tanh(y) + 1.5\tanh(z) \end{aligned}. \tag{21}$$

When model parameters α=1.519, β=-0.04, ρ=-0.5, μ=0.1 and ε=0.45, are fixed, and n=1, a_1=0.02, ω_1=0.08 are chosen, the functions in (20) and (21) are depicted as Fig. 2(c). In Fig. 2(c), there are five intersection points $P_1 - P_5$, and the corresponding equilibrium points can be calculated by using Eqs. (18) and (19). So the five equilibrium points are E_1(-0.1789, -0.389, 1.5929, -0.0087), E_2(-0.205, -0.3696, 1.4435, -0.0082), E_3(0, 0, 0, 0),E_4(0.205, 0.3696, -1.4435, 0.0082), and E_5(0.1789, 0.3897, -1.5929, 0.0087), respectively. The corresponding eigenvalues can be solved by using numerical analysis methods. The numerical results show that E_1 and E_5 have the same eigenvalues λ_1=-0.45, λ_2=-0.8764, $\lambda_3 = \lambda_4$= 0.046 ± 1.366i. E_2 and E_4 have the same eigenvalues λ_1=-0.45, λ_2=-0.833, $\lambda_3 = \lambda_4 = 0.0623 \pm 1.3235i$. And the eigenvalues of E_3 are λ_1=-0.45, λ_2=1.6907, $\lambda_3 = \lambda_4 = -0.4751 \pm 0.8783i$. It is obviously that E_1, E_2, E_4 and E_5 are four unstable saddle focuses, and E_3 is an unstable saddle point. Similarly, when n=2, a_1=0.178, ω_1=0.15, a_2=0.16, and ω_2=0.14 are selected, I_{MLP} has four combinations such as 0.0338, -0.338, 0.018, and -0.018. The corresponding intersection points are plotted in Fig. 2(d). Under this situation, the model (7) has seven equilibrium points. Apparently, the stabilities of all of the equilibrium points can be confirmed by using above analogous analysis methods. It can be proved that when n=2 the model (7) has six unstable saddle focuses and one unstable saddle point. According to the numerical and graphic analysis methods, it can be demonstrated that with the increasing of n, the number of unstable saddle point is not changed, while the number of unstable saddle focus is always equal to $2(n + 1)$. Therefore, the external stimuli can change the number of the equilibrium points in the neural network, which could cause the variation of its dynamics directly. Furthermore, all the equilibrium points in the three models are unstable equilibrium points, which means that the all chaotic attractors generated from the three models are self-excited attractors.

3. Dynamical characteristics of the neural network under different cases

In this section, the dynamical behaviors of the neural network under the three cases are revealed orderly. The numerical researches are carried out by using the four-order Runge-Kutta algorithm with time step h=0.01, and transient period about 2000 time units.

3.1. Simple periodic attractors in case 1

The dynamical phenomena of the model (3) are researched by using phase portraits and Lyapunov exponents. When initial states are kept as (0, 0.1, 0), dynamical trajectory of the neural network without external stimulus on the $x_1 - x_2$ and $x_2 - x_3$ planes is respectively given in Fig. 3(a) and (b). The first three Lyapunov exponents are L_1=0, L_2=-0.6811 and L_3=-0.9185, respectively. As can be seen from Fig. 3, the presented neural network without external stimulus exhibits a periodic attractor.

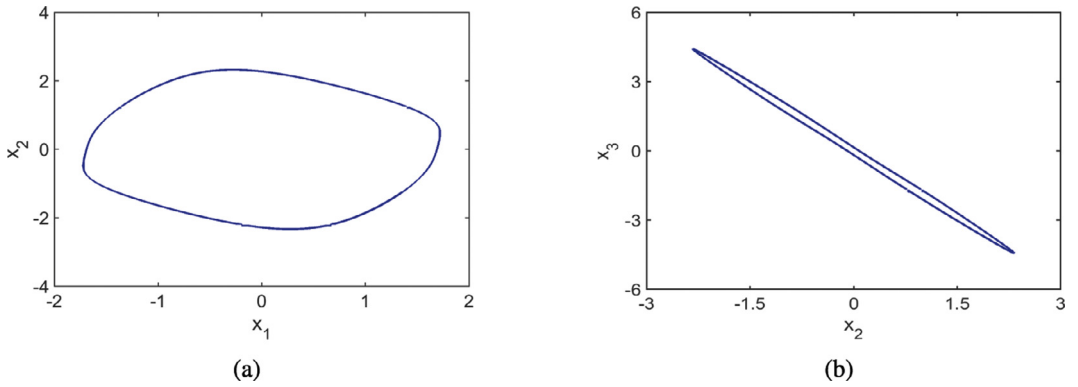

Fig. 3. Periodic attractor of the neural network without external stimulus under initial states (0, 0.1, 0). (a) $x_1 - x_2$ plane, (b) $x_2 - x_3$ plane.

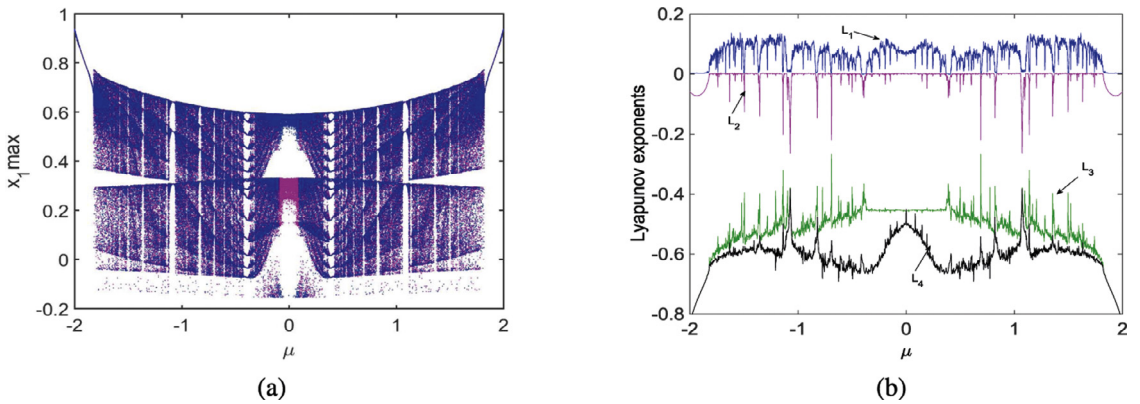

Fig. 4. The μ-dependent dynamics with α=1.519, β=-0.04, ρ=-0.5, ε=0.45. (a) Bifurcation diagram under initial states (0, 0, 0.1, 0) colored in dark blue and (0, 0, -0.1, 0) colored in purple, (b) Lyapunov exponents under initial states (0, 0, 0.1, 0).

3.2. Abundant chaotic attractors in case 2

The chaotic dynamics of the model (5) is analyzed by using bifurcation diagrams, Lyapunov exponents, attraction basin and phase portraits. When the model parameters are fixed as α=1.519, β=-0.04, ρ=-0.5, ε=0.45, and initial states are selected as (0, 0, 0.1, 0) colored in dark blue and (0, 0, -0.1, 0) colored in purple, the μ-parameter bifurcation diagram is plotted in Fig. 4(a). As shown in Fig. 4(a), the dynamical behaviors dependent on the parameter μ are symmetrical about zero value, which is a complex dynamical characteristic. When the adjustable parameter μ increases from -2, orbit of the neural network under electromagnetic radiation begins with period-1limit cycle, then evolves to chaotic behavior at μ=-1.8 by chaos crisis. Thereafter, the orbit breaks into a rich chaotic states until μ=-0.1. As μ increases further, the chaotic behavior develops into coexisting chaotic attractors within the region $\mu \in$ [-0.1, 0]. Interestingly, the neural network begins a reverse dynamical route until μ=2, when μ further increases from 0. Consequently, the neural network affected by electromagnetic radiation presents rich chaotic behaviors in a wide range, i.e., $\mu \in$ [-1.8, 1.8], except some narrow periodic windows like $\mu = \pm 1.58$, $\mu = \pm 1.08$, and $\mu = \pm 0.7$. Furthermore, coexisting chaotic attractors can be detected within the region $\mu \in$ [-0.1, 0.1]. The corresponding first four Lyapunov exponents are drawn as shown in Fig. 4(b). Chaotic attractors of the model (5) with different μ values on $x_1 - x_3$ phase plane are portrayed in Fig. 5. Undoubtedly, the neural network affected by electromagnetic radiation can generate abundant chaotic behaviors.

In addition, to further investigate the coexisting attractors in the neural network under electromagnetic radiation, the attraction basin defined as the domain of initial conditions is depicted. When the adjustable parameter μ is chosen as 0.1, both the initial state $x_2(0)$ and $\varphi(0)$ are fixed as 0, as well as the measureable initial conditions $x_1(0)$ and $x_3(0)$ are scanned in the regions of [-10, 10] and [-10, 10] respectively, the attraction basin in the $x_1(0)$-$x_3(0)$ initial plane is plotted in Fig. 6(a), where purple, yellow, and royal blue regions stand for chaotic attractors with different offset or amplitude. Similarly, when the initial condition $x_1(0)$ and $x_2(0)$ are fixed as 0, the attraction basin in the $x_3(0)$-$\varphi(0)$ initial plane is drawn in Fig. 6(b). The attractors with different topologies are plotted in Fig. 7 under different initial conditions. It is obviously that the neural network affected by electromagnetic radiation exhibits coexisting multiple chaotic attractors, that is, it generates the phenomenon of multistability. Consequently, it can be seen from Figs. 5 and 7 that external electromagnetic radiation can induce plenteous chaotic attractors in the neural network with periodic attractors.

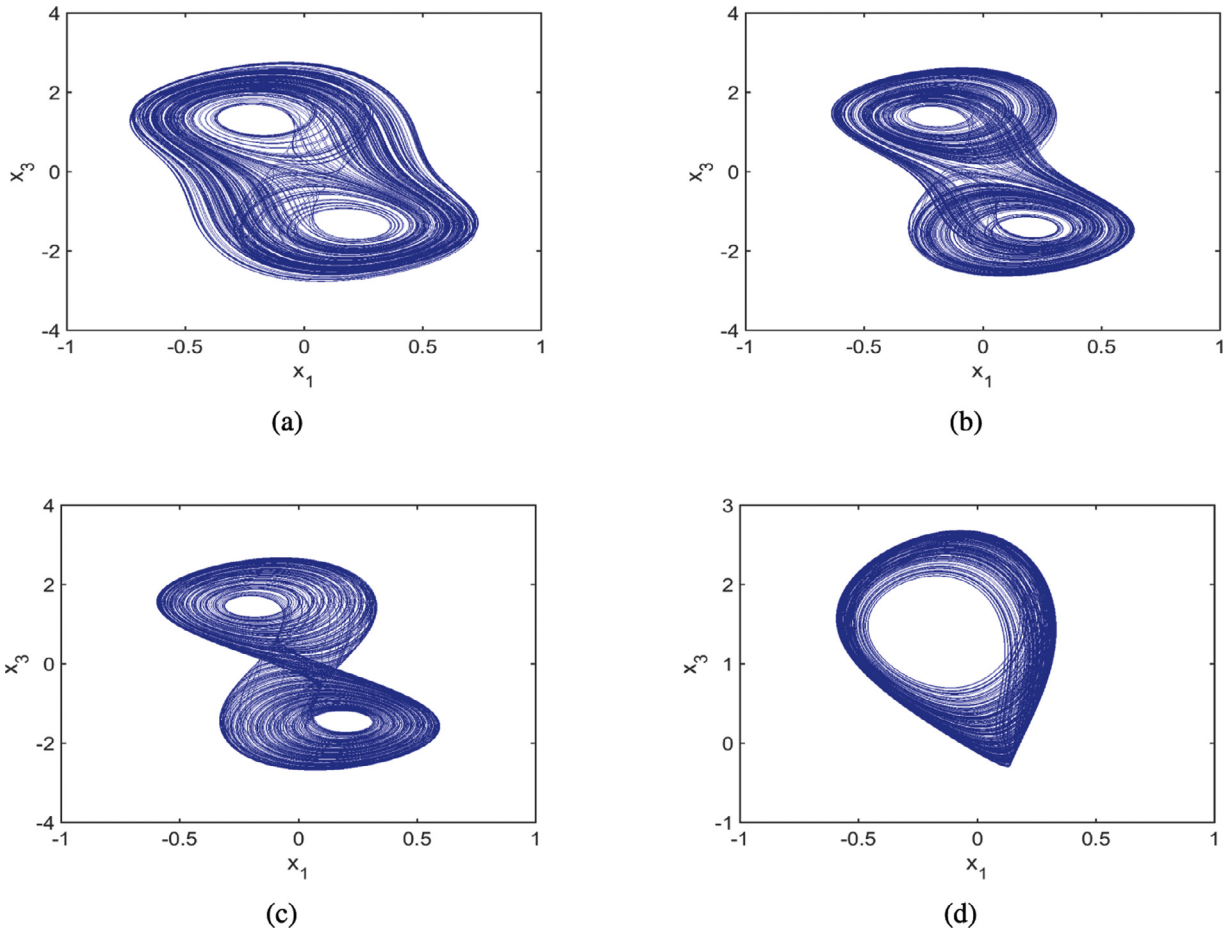

Fig. 5. Chaotic attractors of the neural network under electromagnetic radiation with α=1.519, β=-0.04, ρ=-0.5, ε=0.45, initial states (0, 0, 0.1, 0) and different μ. (a) μ=-1.7, (b) μ =-1, (c) μ=-0.3, (d) μ=-0.1.

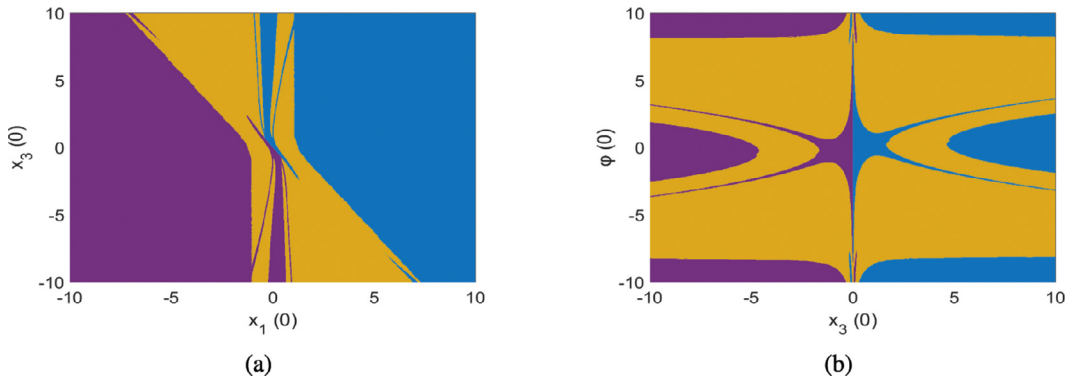

Fig. 6. For adjustable parameter μ=0.1, attraction basins in two initial planes, where purple, yellow, and royal blue regions stand for chaotic attractors with different toplogies. (a) $x_1(0)$-$x_3(0)$ plane, (b) $x_3(0)$-$\varphi(0)$ plane.

3.3. Complex multi-scroll attractors in case 3

Keeping the system parameters α=1.519, β=-0.04, ρ=-0.5, μ=0.1 and ε=0.45, and initial states (0, 0, 0.1, 0) unchanged, the multi-scroll chaotic attractors of the model (7) are explored by using phase portraits, Poincaré maps, and Lyapunov exponents. For example, when n=1, a_1=0.02 and a_2=0.08, the neural network under electromagnetic radiation and multi-level-logic pulse can generate a double-scroll attractor, as shown in Fig. 8a. Meanwhile, the corresponding Poincaré mapping on $x_3 - x_1$ phase plane for the neural network with x_2=0 is depicted in Fig. 8b. It can be seen from Fig. 8b that the

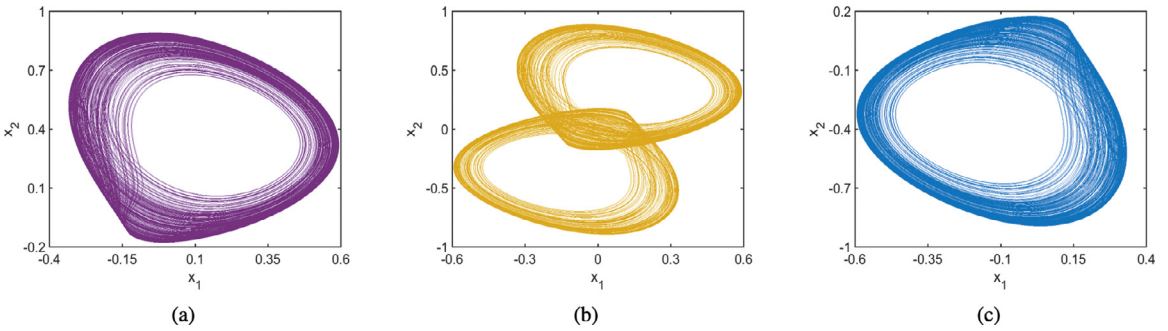

Fig. 7. Coexisting chaotic attractors under different initial conditions. (a) (0,0,-0.1,0) located in purple region, (b) (0,0,5.5,5.5) located in the yellow region, (c) (0,0,0.1,0) located in the royal blue region.

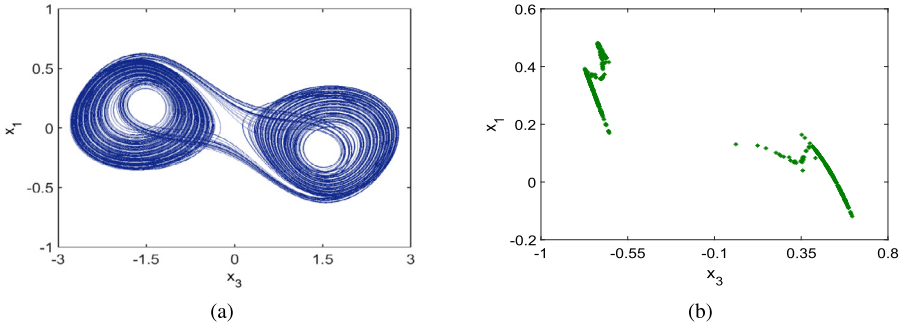

Fig. 8. Double-scroll attractor with $n = 1$, a_1=0.02 and a_2=0.08 and initial states (0,0,0.1,0). (a) Phase portrait, (b) Poincaré mapping.

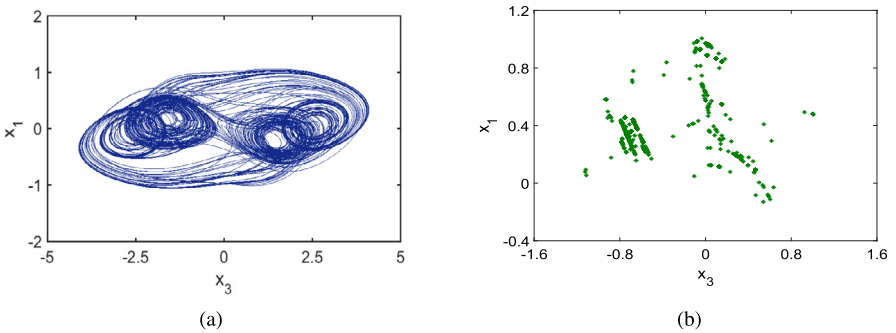

Fig. 9. Four-scroll attractor with n=2, a_1=0.178, ω_1=0.15, a_2=0.16, and ω_2=0.14 and initial states (0,0,0.1,0). (a) Phase portrait (b) Poincaré mapping

Poincaré image contains two irregular open curves, which implies that the double-scroll attractor observed from the neural network is a chaotic attractor. Moreover, the corresponding first four Lyapunov exponents are L_1=0.025, L_2=0, L_3=-0.4585, L_4=-0.7141, respectively.

When n=2, a_1=0.178, ω_1=0.15, a_2=0.16, and ω_2=0.14, a four-scroll attractor can be detected in the model (7), as shown in Fig. 9(a). And its first four Lyapunov exponents are L_1=0.0627, L_2=0, L_3=-0.4621, L_4=-0.7812, respectively. The Poincaré mapping on $x_3 - x_1$ phase plane for the neural network with x_2=0 is depicted in Fig. 9(b). In Fig. 9(b), the Poincaré image exhibits a patch of irregular dense points, which means that the neural network affected by electromagnetic radiation and electric pulse produce complex four-scroll chaotic attractors.

Similarly, when n=3, a_1=0.24, ω_1=0.25, a_2=0.31, ω_2=0.21, a_3=0.5, and ω_3=0.14, a six-scroll attractor can be observed in the model (7), as shown in Fig. 10(a). Under this case, the first four Lyapunov exponents are L_1=0.0627, L_1=-0.1479, L_1=-0.2588, L_1=-0.6761, respectively. And the Poincare mapping on $x_2 - \varphi$ phase plane for the neural network with x_2=0 is drawn in Fig. 10(b). Clearly, the six-scroll attractor is a complex chaotic attractor due to the Poincaré image displays a patch of irregular dense points. It is obviously that chaotic attractor can be switched to multi-scroll attractor by simultaneously injecting external electromagnetic radiation and multi-level-logic pulse in the neural network. Such multi-scroll attractor has not been found yet in the previously reported Hopfield neural networks. It is also found that the number of generated scrolls

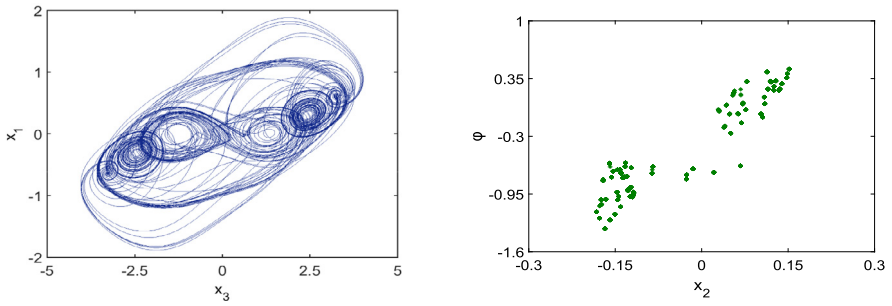

Fig. 10. Six-scroll attractor with n=3, a_1=0.24, ω_1=0.25, a_2=0.31, ω_2=0.21, a_3=0.5, and ω_3=0.14 and initial states (0,0,0.1,0). (a) Phase portrait, (b) Poincaré mapping

depends on the number of available electric pulse, which can be realized by using the different pulse-exciting combinations. Hence, more numbers of scrolls can be achieved by selecting the different pulse combinations in the model (7).

4. Hamilton energy analysis and discussion

It is extremely significant to explore energy release and capture during the transition of dynamical behavior in neural network, because the occurrence and transition of electric activities of neurons depend on the energy release and supply [59,60]. Based on the Helmholtz theorem [55], any velocity vector field can be considered as a sum of the conservative field containing the full rotation and the dissipative field containing the divergence. As a consequence, for a general continuous nonlinear dynamical system $F(x)$, its dynamical equations can be expressed by the follow form:[57,58]

$$F(x) = F_c(x) + F_d(x) = [J(x) + R(x)]\nabla H, \tag{22}$$

where $F_c(x)$ and $F_d(x)$ are the conservative field and the dissipative field, respectively. ΔH is the gradient vector of a smooth energy function $H(x)$.$J(x)$ and $R(x)$ are a skew-symmetric matrix and a symmetric matrix, respectively. Then the Hamilton energy function can be approached by

$$\begin{cases} \dot{H} = \nabla H^T R(x)\nabla H = \nabla H^T F_d(x) \\ \nabla H^T J(x)\nabla H = \nabla H^T F_c(x) = 0 \end{cases} \tag{23}$$

Thus, for the neural network in model (3), one has

$$F_c(x) = \begin{bmatrix} 2\tanh(x_2) + 0.9\tanh(x_3) \\ -1.5\tanh(x_1) - 0.45\tanh(x_3) \\ 3\tanh(x_1) - 2\tanh(x_2) \end{bmatrix}, \tag{24}$$

$$F_d(x) = \begin{bmatrix} -x_1 + 1.5\tanh(x_1) \\ -x_2 + 1.5\tanh(x_2) \\ -x_3 + 1.5\tanh(x_3) \end{bmatrix}. \tag{25}$$

According to Eqs. (22) and (23), the Hamilton energy function $H(x_1, x_2, x_3)$ of the neural network can be written as follows:

$$\frac{\partial H}{\partial x_1}(2\tanh(x_2) + 0.9\tanh(x_3)) - \frac{\partial H}{\partial x_2}(1.5\tanh(x_1) + 0.45\tanh(x_3)) + \frac{\partial H}{\partial x_3}(3\tanh(x_1) - 2\tanh(x_2)) = 0. \tag{26}$$

Afterwards, a general solution of Eq. (26) is given by

$$H = x_1 + 2x_2 + x_3. \tag{27}$$

Moreover, the differential versus time of the Hamilton energy function can be calculated by

$$\begin{aligned} dH/dt &= dx_1/dt + 2dx_2/dt + dx_3/dt \\ &= -x_1 - 2x_2 - x_3 + 1.5\tanh(x_1) + 3\tanh(x_2) + 1.5\tanh(x_3). \\ &= \nabla H^T F_d(x) \end{aligned} \tag{28}$$

Evidently, the Hamilton energy function in Eq. (27) satisfies the condition as shown in Eq. (23). According to references [68,69], it should be pointed that the Hamilton energy functions should be independent of the external forcing term. That is to say, the models (5) and (7) have the same Hamilton energy function as the neural network model (3).

According to Eq. (27), the Hamilton energy function is mainly dependent on the membrane potential of three neurons in the neural network. That is, the Hamilton energy of the neural network is directly related to its dynamical behaviors instead of external stimuli. Thus, it is important to observe the evolution of Hamilton energy by inducing different attractors in the

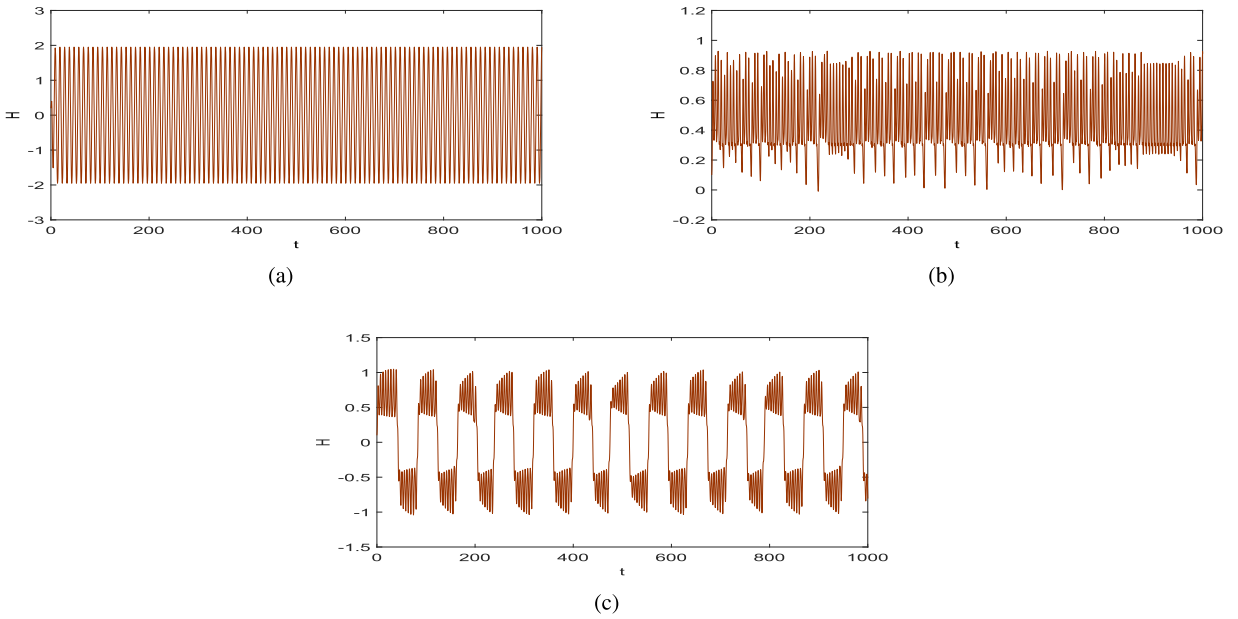

Fig. 11. Evolution of Hamilton energy in the neural network under different cases. (a) periodic attractor in case1, (b) chaotic attractor in case 2 with μ=0.1, (c) double-scroll attractor in case 3.

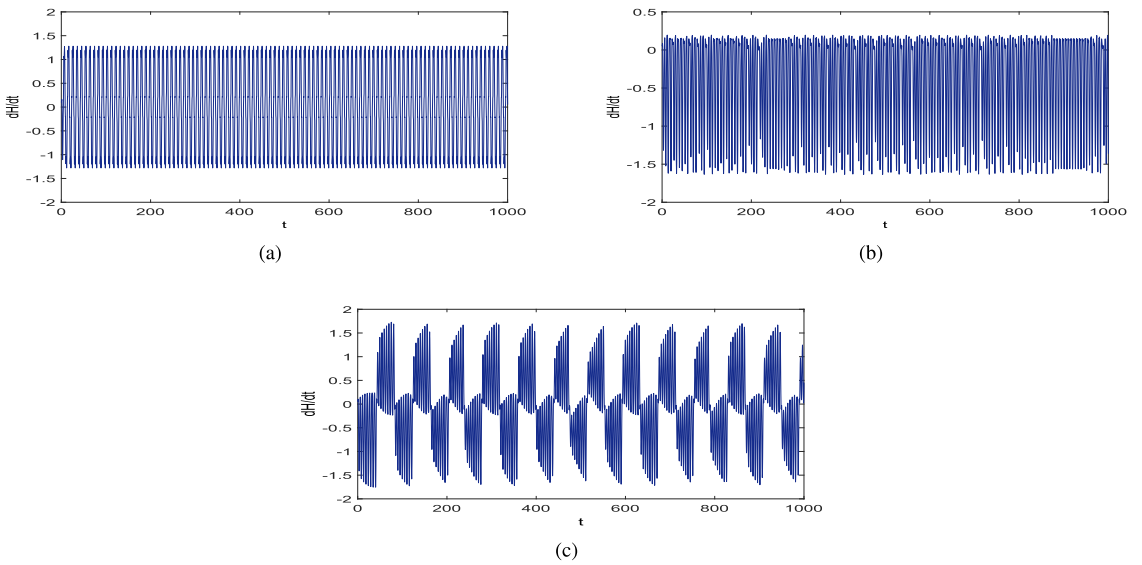

Fig. 12. Hamilton energy derivative for the neural network under different cases. (a) periodic attractor in case1, (b) chaotic attractor in case 2 with μ=0.1, (c) double-scroll attractor in case 3.

neural network under different external stimulus, and the detailed results are plotted in Fig. 11. Fig. 11(a) shows the evolution of the Hamilton energy of the periodic attractor in the neural network without any external stimulus. Fig. 11(b) shows the evolution of the energy of the chaotic attractor in the neural network stimulated by electromagnetic radiation. Fig. 11(c) presents the evolution of the energy of the double-scroll attractor in the neural network under electromagnetic radiation and multi-level-logic pulse. As depicted in Fig. 11, the neural network has the different energy consumption and release periods with respect to the different attractors. Hence, we believe that the energy distributions are mainly dependent on its dynamical behaviors in the neural system. As it can also be seen, in the case of the periodic attractor, the Hamilton energy fluctuates with higher amplitude than in the case of the chaotic attractor and the double-scroll attractor. In other words, external stimulus shrinks the fluctuation of Hamilton energy in the neural network indirectly and greatly. Furthermore, the corresponding Hamilton energy derivative is given in Fig. 12. As shown in Fig. 12, the neural network in the cases 1 and 3 exhibit intermittent release and absorbing in energy, while in the case 2 always consumes energy.

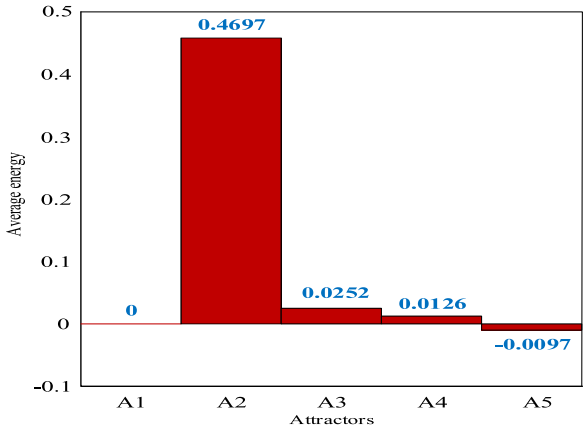

Fig. 13. Development of average Hamilton energy in the neural network, calculated by changing the external stimuli, and the average time for the calculations T=2000 time units.

To further estimate the dependence of Hamilton energy on dynamical behaviors of the neural network, the average Hamilton energy is calculated by

$$< H >= \frac{1}{T}\int_{T_0}^{T_0+T} H(x_1, x_2, x_3)dt, \tag{29}$$

where T_0 is the beginning time and T is the calculation period about 2000 time units. By changing the external stimulus, the evolution of average Hamilton energy is calculated, as shown in the bar chart Fig. 13, where $A_1 - A_5$ denote periodic attractor in case 1, chaotic attractor in case 2, double-scroll attractor in case 3, four-scroll attractor in case 3, and six-scroll attractor in case 3, respectively. As shown in Fig. 13, the average Hamilton energy of the periodic attractor in the neural network without external stimulus is zero due to energy conservation effect. Interestingly, the average energy of the neural network undergoes a rapid jump when its dynamical behavior is switched from the periodic attractor to the chaotic attractor. This result is mainly due to the input of external electromagnetic radiation (energy). However, the average energy in the neural network decreases greatly with the increase of the number of scrolls. The potential mechanism could be that more complex external stimulation can much contribute to the multi-scroll behaviors in the neural system. It means that external stimuli can decrease the energy cost triggering for dynamical behaviors of the neural network. Moreover, the results in Fig. 13 confirm that continuous release and absorbing in energy can obtain a lower average Hamilton energy in the neural system. As a result, appropriate external stimuli can enhance chaotic behaviors and also decrease the Hamilton energy.

5. Hardware experiments

The circuital realization of the mathematical model is extremely vital and necessary to the practical engineering applications [70]. As a rule, nonlinear dynamical equations can be physically implemented by employing already existing electric elements like resistors, capacitors, operational amplifiers and analog multipliers [64,71]. Thus, the neural circuit can be designed and manufactured in real life, which means that the theoretical and numerical results of the neural network model can be effectively demonstrated by hardware experiments.

5.1. Physical circuit design

Before realizing the neural circuit, we first introduce a hyperbolic tangent function circuit [63] and a multi-level-logic pulse function circuit [52], as shown in Fig. 14. In Fig. 14(a), when R=10$k\Omega$, R_F=520Ω, R_C=1$k\Omega$ and I_o=1.1mA, the input-output relationship of the hyperbolic tangent circuit can be expressed by V_o=-tanh(V_i). And in Fig. 14(b), when R_S=13.5$k\Omega$, R_K=1$k\Omega$ and V_{sn}= sin(2πFt), the output current can be calculated by I_{MLP}=sign(sin(2πFnt))/R_{An}. Considering the models (3), (5) and (7), the neural circuit is designed in Fig. 15. It is noted that two switches are added in the neural circuit to control the different external stimuli. According to Kirchhoff circuit law, the corresponding circuit state equations are given by

$$\begin{cases} RC\frac{dv_1}{dt} = -v_1 + \frac{R}{R_1}\tanh(v_1) + \frac{R}{R_2}\tanh(v_2) + \frac{R}{R_3}\tanh(v_3) \\ RC\frac{dv_2}{dt} = -v_2 - \frac{R}{R_4}\tanh(v_1) + \frac{R}{R_5}\tanh(v_2) - \frac{R}{R_6}\tanh(v_3), \\ RC\frac{dv_3}{dt} = -v_3 + \frac{R}{R_7}\tanh(v_1) - \frac{R}{R_8}\tanh(v_2) + \frac{R}{R_9}\tanh(v_3) \end{cases} \tag{30}$$

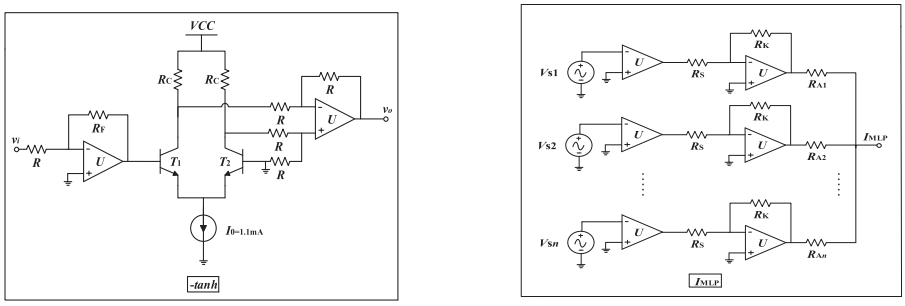

(a) (b)

Fig. 14. Circuit implementation of hyperbolic tangent function and multi-level-logic pulse function.(a)Hyperbolic tangent function unit, (b) multi-level-logic pulse unit.

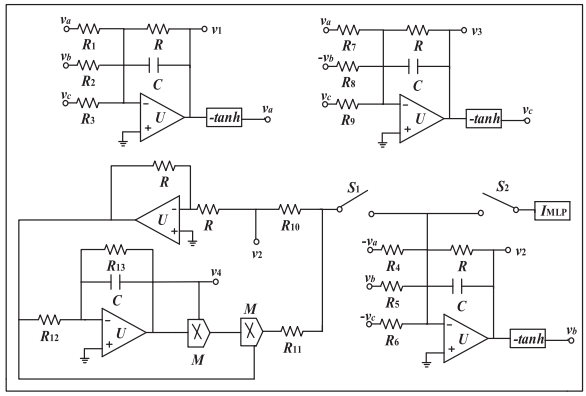

Fig. 15. Main circuit structure of the neural network under different external stimuli.

$$\begin{cases} RC\frac{dv_1}{dt} = -v_1 + \frac{R}{R_1}\tanh(v_1) + \frac{R}{R_2}\tanh(v_2) + \frac{R}{R_3}\tanh(v_3) \\ RC\frac{dv_2}{dt} = -v_2 - \frac{R}{R_4}\tanh(v_1) + \frac{R}{R_5}\tanh(v_2) - \frac{R}{R_6}\tanh(v_3) + Rv_2(-\frac{1}{R_{10}} + \frac{{v_4}^2}{R_{11}}) \\ RC\frac{dv_3}{dt} = -v_3 + \frac{R}{R_7}\tanh(v_1) - \frac{R}{R_8}\tanh(v_2) + \frac{R}{R_9}\tanh(v_3) \\ RC\frac{dv_4}{dt} = \frac{R}{R_{12}}v_2 - \frac{R}{R_{13}}v_4 \end{cases}, \tag{31}$$

$$\begin{cases} RC\frac{dv_1}{dt} = -v_1 + \frac{R}{R_1}\tanh(v_1) + \frac{R}{R_2}\tanh(v_2) + \frac{R}{R_3}\tanh(v_3) \\ RC\frac{dv_2}{dt} = -v_2 - \frac{R}{R_4}\tanh(v_1) + \frac{R}{R_5}\tanh(v_2) - \frac{R}{R_6}\tanh(v_3) + Rv_2(-\frac{1}{R_{10}} + \frac{{v_4}^2}{R_{11}}) + I_{MLP} \\ RC\frac{dv_3}{dt} = -v_3 + \frac{R}{R_7}\tanh(v_1) - \frac{R}{R_8}\tanh(v_2) + \frac{R}{R_9}\tanh(v_3) \\ RC\frac{dv_4}{dt} = \frac{R}{R_{12}}v_2 - \frac{R}{R_{13}}v_4 \end{cases}, \tag{32}$$

where RC is the integral time constant, and v_1, v_2, v_3, v_4 are the voltages on the capacitors of four integral circuits, respectively. Besides, $-v_a$, $-v_b$ and $-v_c$ can be realized by inverting amplifiers. Assuming that RC=10us, the resistance R=10$k\Omega$, then the C can be chosen as 1nF. In view of the coefficient of the neural network model and error influence, part resistances can be calculated as R_1=6.67$k\Omega$, R_2= 5$k\Omega$, R_3=11$k\Omega$, R_4 = R_5=6.67$k\Omega$, R_6=22$k\Omega$, R_7=3.5$k\Omega$, R_8=5$k\Omega$, R_9=7$k\Omega$. Furthermore, the adjustable resistors $R_{An} = R/a_n$, $R_{10} = R/\rho\alpha$, $R_{11} = g^2R/3\beta\rho$, $R_{12} = R/\mu$, $R_{13} = R/\varepsilon$, and $F_n = \omega_n/2\pi RC$, where g=0.1 is the control gain of the multiplier M.

5.2. Hardware circuit experiments

The neural circuit given in Fig. 15 is implemented on the experimental circuit breadboard through adopting electrical elements including metal resistors, precision potentiometers, ceramic capacitors, operational amplifiers TL082CP and analog multipliers AD633JN, as shown in Fig. 16. Among them, TL082CP and AD633JN are supplied by ± 15V voltage sources. And the sinusoidal voltage sources are achieved by function generators, and the experimental results are measured by an analog

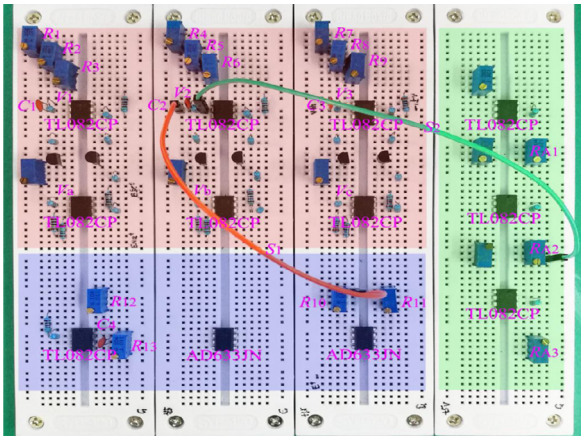

Fig. 16. The photo of the hardware circuit of the neural network under different external stimuli.

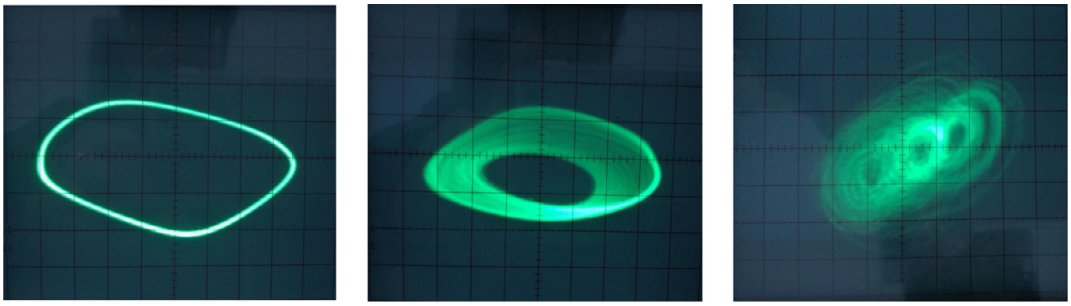

(a) (b) (c)

Fig. 17. Experimental results in the neural network under different external stimuli. (a) Periodic attractor under case 1, (b) Chaotic attractor under case 2, (c) Four-scroll attractor under case 3.

oscilloscope. After that, the numerical results given in the Section 3 are experimentally proved by selecting appropriate switches.

(1) When S_1 and S_2 are opened, the circuit of the model (3) can be realized. The periodic attractor can be generated from the neural circuit, as shown in Fig. 17(a).
(2) When S_1 is closed and S_2 is opened, the circuit of the model (5) can be established. Regarding the system parameters α=1.519, β=-0.04, ρ=-0.5, μ=0.1 and ε=0.45, the corresponding resistances are chosen as R_{10}=12.5$k\Omega$, R_{11}=2$k\Omega$, R_{12}=100$k\Omega$, R_{13}=21.4$k\Omega$, and the single scroll chaotic attractor can be captured from the neural circuit, as shown in Fig. 17(b).
(3) When S_1 and S_2 are closed, the circuit of the model (7) can be completed. For n=2, a_1=0.178, ω_1=0.15, a_2=0.16 and ω_2=0.14, the circuit parameters are selected as F_1=2389Hz, F_2=2230Hz, R_{A1}=56.18$k\Omega$, R_{A2}=62.5$k\Omega$, and the four-scroll attractor can be captured as shown in Fig. 17(c).

6. Conclusions

Chaotic dynamics in a neural network under different external stimuli is studied in this paper. The neural network under three different cases, namely, without external stimulation, with electromagnetic radiation stimulation, and with both electromagnetic radiation and multi-level-logic pulse stimulations are mathematically modeled. The research results show that the three-neurons-based neural network with periodic attractors can induce rich chaotic behaviors including coexisting chaotic attractors when its one neuron is stimulated by external electromagnetic radiation. And, the multi-scroll chaotic attractors like double-scroll attractors, four-scroll attractors and six-scroll attractors can be observed in the neural network simultaneously stimulated by electromagnetic radiation and multi-level-logic pulse. Furthermore, the Hamilton energy function is calculated to find the energy changes when different external stimuli is imposed on the neural network. It is also found that external stimuli can decrease the energy cost inducing more complex dynamical behaviors in the neural network. Hardware experimental results demonstrate the theoretical and numerical results, effectively. These results may have potential applications in the diagnosis and therapy of neurological diseases.

Declaration of Competing Interest

The authors declare that they have no known competing financial interests or personal relationships that could have appeared to influence the work reported in this paper.

CRediT authorship contribution statement

Chunhua Wang: Data curation, Writing - original draft, Conceptualization, Methodology. **Wei Yao:** Visualization, Investigation. **Yumei Tan:** Writing - review & editing.

Acknowledgments

This project is supported by The Major Research Project of National Natural Science Foundation of China (No. 91964108), The National Natural Science Foundation of China (No. 61971185) and The Open Fund Project of Key Laboratory in Hunan Universities (No. 18K010).

References

[1] Sporns O, Tononi G, Edelman GM. Connectivity and complexity: the relationship between neuroanatomy and brain dynamics. Neural Netw 2000;13(8–9):909–22.
[2] Wang H, Lu Q, Wang Q. Bursting and synchronization transition in the coupled modified ML neurons. Commun Nonlinear Sci Numer Simul 2008;13(8):1668–75.
[3] Ma J, Tang J. A review for dynamics in neuron and neuronal network. Nonlinear Dyn 2017;89(3):1569–78.
[4] Kwan P, Brodie MJ. Early identification of refractory epilepsy. N Engl J Med 2000;342(5):314–19.
[5] Villoslada P, Steinman L, Baranzini SE. Systems biology and its application to the understanding of neurological diseases. Ann Neurol 2009;65(2):124–39.
[6] de H W, van FWM, Koene T, et al. Disrupted modular brain dynamics reflect cognitive dysfunction in alzheimer's disease. Neuroimage 2012;59(4):3085–93.
[7] Yu F, Liu L, Xiao L, et al. A robust and fixed-time zeroing neural dynamics for computing time-variant nonlinear equation using a novel nonlinear activation function. Neurocomputing 2019;350:108–16.
[8] Yao W, Wang C, Cao J, et al. Hybrid multisynchronization of coupled multistable memristive neural networks with time delays. Neurocomputing 2019;363:281–94.
[9] Chen Y, Wang J, Xia R, et al. The visual object tracking algorithm research based on adaptive combination kernel. J Ambient Intell Humaniz Comput 2019:1–13.
[10] Bashkirtseva I, Nasyrova V, Ryashko L. Analysis of noise effects in a map-based neuron model with canard-type quasiperiodic oscillations. Commun Nonlinear Sci Numer Simul 2018;63:261–70.
[11] Zhou C, Wang C, Sun Y, Yao W. Weighted sum synchronization of memristive coupled neural networks. Neurocomputing 2020;4:225–32.
[12] Jin J, Zhao L, Li M, et al. Improved zeroing neural networks for finite time solving nonlinear equations. Neural Comput Appl 2020;32(9):4151–60.
[13] Zhang X, Wang C, Yao W, et al. Chaotic system with bondorbital attractors. Nonlinear Dyn 2019;97(4):2159–74.
[14] Zhou L, Wang C, Du S, et al. Cluster synchronization on multiple nonlinearly coupled dynamical subnetworks of complex networks with nonidentical nodes. IEEE Trans Neural Netw Learn Syst 2016;28(3):570–83.
[15] Kumar S, Strachan JP, Williams RS. Chaotic dynamics in nanoscale nbo 2 mott memristors for analogue computing. Nature 2017;548(7667):318–21.
[16] Huang J, Fu X. Stability and chaos for an adjustable excited oscillator with system switch. Commun Nonlinear Sci Numer Simul 2019;77:108–25.
[17] Pham VT, Jafari S, Kapitaniak T, et al. Generating a chaotic system with one stable equilibrium. Int J Bifurcation Chaos 2017;27(04):1750053.
[18] Cang S, Li Y, Zhang R, et al. Hidden and self-excited coexisting attractors in a lorenz-like system with two equilibrium points. Nonlinear Dyn 2019;95(1):381–90.
[19] Kengne J. Coexistence of chaos with hyperchaos, period-3 doubling bifurcation, and transient chaos in the hyperchaotic oscillator with gyrators. Int J Bifurcation Chaos 2015;25(04):1550052.
[20] He S, Sun K, Wang H. Dynamics and synchronization of conformable fractional-order hyperchaotic systems using the homotopy analysis method. Commun Nonlinear Sci Numer Simul 2019;73:146–64.
[21] Hua Z, Yi S, Zhou Y, et al. Designing hyperchaotic cat maps with any desired number of positive lyapunov exponents. IEEE Trans cybernetics 2017;48(2):463–73.
[22] Jafari S, Pham VT, Kapitaniak T. Multiscroll chaotic sea obtained from a simple 3d system without equilibrium. Int J Bifurcation Chaos 2016;26(02):1650031.
[23] Wang N, Li C, Bao H, et al. Generating multi-scroll chua's attractors via simplified piecewise-linear chua's diode. IEEE Trans Circuits Syst I 2019;66(12):4767–79. Reg. Papers
[24] Zhang X, Wang C. Multiscroll hyperchaotic system with hidden attractors and its circuit implementation. Int J Bifurcation Chaos 2019;29(09). 1950117
[25] Tlelo-Cuautle E, Rangel-Magdaleno JJ, Pano-Azucena AD, et al. FPGA Realization of multi-scroll chaotic oscillators. Commun Nonlinear Sci Numer Simul 2015;27(1–3):66–80.
[26] Zhao Q, Wang C, Zhang X. A universal emulator for memristor, memcapacitor, and meminductor and its circuit. Chaos 2019;29(1):013141.
[27] Zhang X, Wang C. A novel multi-attractor period multi-scroll chaotic integrated circuit based on CMOS wide adjustable CCCII. IEEE Access 2019;7:16336–50.
[28] Yu S, Lu J, Leung H, Papers R, et al. Design and implementation of n-scroll chaotic attractors from a general jerk circuit. IEEE Trans Circuits Syst I 2005;52(7):1459–76.
[29] Hu X, Liu C, Liu L, et al. Multi-scroll hidden attractors in improved sprott a system. Nonlinear Dyn 2016;86(3):1725–34.
[30] Hong Q, Xie Q, Shen Y, et al. Generating multi-double-scroll attractors via nonautonomous approach. Chaos 2016;26(8):083110.
[31] Wang C, Liu X, Xia H. Multi-piecewise quadratic nonlinearity memristor and its 2 n-scroll and 2 n+ 1-scroll chaotic attractors system. Chaos 2017;27(3):033114.
[32] Hopfield JJ. Neurons with graded response have collective computational properties like those of two-state neurons. Proc Natl Acad Sci U S A 1984;81(10):3088–92.
[33] Chen J, Li K, Bilal K, et al. A bi-layered parallel training architecture for large-scale convolutional neural networks. IEEE Trans Parallel Distrib Syst 2018;30(5):965–76.
[34] Huang WZ, Huang Y. Chaos of a new class of hopfield neural networks. Appl Math Comput 2008;206(1):1–11.
[35] Zheng P, Tang W, Zhang J. Dynamic analysis of unstable hopfield networks. Nonlinear Dyn 2010;61(3):399–406.

[36] Bao B, Qian H, Wang J, et al. Numerical analyses and experimental validations of coexisting multiple attractors in hopfield neural network. Nonlinear Dyn 2017;90(4):2359–69.
[37] Xu Q, Song Z, Qian H, et al. Numerical analyses and breadboard experiments of twin attractors in two-neuron-based non-autonomous hopfield neural network. Eur Phys J-Spec Top 2018;227(7–9):777–86.
[38] Bao B, Chen C, Bao H, et al. Dynamical effects of neuron activation gradient on hopfield neural network: numerical analyses and hardware experiments 2019;29(04):):1930010.
[39] Rech PC. Chaos and hyperchaos in a hopfield neural network. Neurocomputing 2011;74(17):3361–4.
[40] Danca MF, Kuznetsov N. Hidden chaotic sets in a hopfield neural system. Chaos Solitons Fractals 2017;103:144–50.
[41] Bao B, Qian H, Xu Q, et al. Coexisting behaviors of asymmetric attractors in hyperbolic-type memristor based hopfield neural network. Frontiers in computational neuroscience 2017;11. 81–81
[42] Chen C, Chen J, Bao H, et al. Coexisting multi-stable patterns in memristor synapse-coupled hopfield neural network with two neurons. Nonlinear Dyn 2019;95(4):3385–99.
[43] Chen C, Bao H, Chen M, et al. Non-ideal memristor synapse-coupled bi-neuron hopfield neural network: numerical simulations and breadboard experiments. AEU-Int J Electron Commun 2019;111:152894.
[44] Li Q, Tang S, Zeng H, et al. On hyperchaos in a small memristive neural network. Nonlinear Dyn 2014;78(2):1087–99.
[45] Pham VT, Jafari S, Vaidyanathan S, et al. A novel memristive neural network with hidden attractors and its circuitry implementation. Sci China-Technol Sci 2016;59(3):358–63.
[46] Li J, Liu S, Liu W, et al. Suppression of firing activities in neuron and neurons of network induced by electromagnetic radiation. Nonlinear Dyn 2016;83(1–2):801–10.
[47] Etémé AS, Tabi CB, Mohamadou A. Firing and synchronization modes in neural network under magnetic stimulation. Commun Nonlinear Sci Numer Simul 2019;72:432–40.
[48] Tabi CB, Etémé AS, Mohamadou A, Kofané TC. Unstable discrete modes in hindmarsh-rose neural networks under magnetic flow effect. Chaos Solitons Fractals 2019;123:116–23.
[49] Etémé AS, Tabi CB, Mohamadou A, Kofané TC. Elimination of spiral waves in a two-dimensional hindmarsh-rose neural network under long-range interaction effect and frequency excitation. Physica A-Statistical Mechanics and Its Applications 2019;533:122037.
[50] Etémé AS, Tabi CB, Mohamadou A, Kofané TC. Long-range memory effects in a magnetized hindmarsh-rose neural network. Commun Nonlinear Sci Numer Simul 2020;84:105208.
[51] Ma J, Zhang G, Hayat T, et al. Model electrical activity of neuron under electric field. Nonlinear Dyn 2019;95:1585–98.
[52] Bao H, Hu A, Liu W. Bipolar pulse-induced coexisting firing patterns in two-dimensional hindmarshrose neuron model. Int J Bifurcation Chaos 2019;29(01):1950006.
[53] Zhu Z, Wang R, Zhu F. The energy coding of a structural neural network based on the hodgkin-huxley model. Front Neurosci 2018;12:122.
[54] Lin H, Wang C, Sun Y, w Y. Firing multistability in a locally active memristive neuron model. Nonlinear Dyn 2020. doi:10.1007/s11071-020-05687-3.
[55] Kobe DH. Helmholtz'S theorem revisited. Am J Phys 1986;54(6):552–4.
[56] Li F, Yao C. The infinite-scroll attractor and energy transition in chaotic circuit. Nonlinear Dyn 2016;84(4):2305–15.
[57] Ma J, Wu F, Jin W, et al. Calculation of hamilton energy and control of dynamical systems with different types of attractors. Chaos 2017;27(5):053108.
[58] Xin A, Li Z. Dynamics analysis and hamilton energy control of a generalized lorenz system with hidden attractor. Nonlinear Dyn 2018;94(4):2995–3010.
[59] Xin LS, Wu YJ, Jun M. Energy dependence on the electric activities of a neuron. Chin Phys B 2015;24(12):128710.
[60] Wang Y, Wang C, Ren G, et al. Energy dependence on modes of electric activities of neuron driven by multi-channel signals. Nonlinear Dyn 2017;89(3):1967–87.
[61] Wu FQ, Ma J, Zhang G. Energy estimation and coupling synchronization between biophysical neurons. Sci China-Technol Sci 2019:1–12.
[62] Hu X, Liu C, Liu L, et al. Chaotic dynamics in a neural network under electromagnetic radiation. Nonlinear Dyn 2018;91(3):1541–54.
[63] Lin H, Wang C, Tan Y. Hidden extreme multistability with hyperchaos and transient chaos in a hopfield neural network affected by electromagnetic radiation. Nonlinear Dyn 2020;99(3):2369–86.
[64] Lin H, Wang C. Influences of electromagnetic radiation distribution on chaotic dynamics of a neural network. Appl Math Comput 2020;369:124840.
[65] Wang C, Xiong L, Sun J, et al. Memristor-based neural networks with weight simultaneous perturbation training. Nonlinear Dyn 2019;95(4):2893–906.
[66] Lv M, Ma J. Multiple modes of electrical activities in a new neuron model under electromagnetic radiation. Neurocomputing 2016;205:375–81.
[67] Ge M, Jia Y, Xu Y, et al. Mode transition in electrical activities of neuron driven by high and low frequency stimulus in the presence of electromagnetic induction and radiation. Nonlinear Dyn 2018;91(1):515–23.
[68] Torrealdea FJ, Sarasola C, d'Anjou A. Energy consumption and information transmission in model neurons. Chaos Solitons Fractals 2009;40(1):60–8.
[69] Moujahid A, d'Anjou A, Torrealdea FJ, et al. Efficient synchronization of structurally adaptive coupled hindmarsh-rose neurons. Chaos Solitons Fractals 2011;44(11):929–33.
[70] Duan S, Hu X, Dong Z, et al. Memristor-based cellular nonlinear/neural network: design, analysis, and applications. IEEE Trans Neural Netw Learn Syst 2014;26(6):1202–13.
[71] Kengne J, Jafari S, Njitacke ZT, et al. Dynamic analysis and electronic circuit implementation of a novel 3d autonomous system without linear terms. Commun Nonlinear Sci Numer Simul 2017;52:62–76.